SPATIAL DOMAIN FILTERING OF SPECKLE INTERFEROGRAMS DEPICTING VIBRATION MODES

Florin GAROI[1], Paul ŞCHIOPU[2] and Dan APOSTOL[3]

În această lucrare investigăm îmbunătățirea interferogramelor în lumină granulară obținute prin Digital Speckle Pattern Interferometry (DSPI) din vibrația unei plăci de aluminiu cu frecvențele proprii de 3.05, 4.18 şi 4.56 kHz. Folosind un algoritm propriu, am obținut o îmbunătățire a raportului semnal/zgomot de 0.3, 0.5 şi respectiv 0.3 pentru cele trei cazuri studiate. Se aplică egalizarea histogramei pentru îmbunătățirea contrastului şi intervalului dinamic.

In this paper we investigate the improvement of speckle interferograms obtained with Digital Speckle Pattern Interferometry (DSPI) from vibration of an aluminium plate with 3.05, 4.18 and 4.56 kHz frequencies. With our algorithm, we obtained a SNR improvement of 0.3, 0.5 and 0.35 respectively for the three studied cases. Histogram equalization is applied to improve both the contrast and dynamic range.

Keywords: image processing, speckle interferometry, histogram, median filter, Gaussian filter, vibration, measurement

1. Introduction

Vibration monitoring and measurement is of great importance in discovering possible problems associated with machines and various structures as well as in controlling their noise level. Digital Speckle Pattern Interferometry (DSPI) is a full field, non-contact and real time technique to measure the vibrations of optically rough structures [1-7]. It is well-known that all speckle interferograms obtained need processing [5-13] after recording. Even though the method has many advantages, its main drawback is poor images. However, image processing tool successfully covers this aspect.

In the present work we investigate vibrations of an aluminium plate. Vibrations modes of this plate are shown and recorded as speckle interferograms. Using a personal algorithm we successfully improve the *SNR* of these images.

[1] Research scientist., Laser Depart., National Institute for Lasers, Plasma and Radiation Physics, Bucharest, Romania, e-mail: florin.garoi@inflpr.ro
[2] Prof., Optoelectronics Depart., POLITEHNICA University of Bucharest, Romania, e-mail: schiopu.paul@yahoo.com
[3] PhD, Laser Depart., National Institute for Lasers, Plasma and Radiation Physics, Bucharest, Romania, e-mail: dan.apostol@inflpr.ro

2. Experimental setup and the speckle interferograms

A DSPI setup (Fig. 1) was realized to analyze vibrations of a square aluminium plate (144.5 × 144.5 × 1 mm). The arrangement is a Mach-Zender interferometer and the fringes are visualized and recorded on a computer via a Baxal CCD camera. Vibrations in the plate are induced by a shaker, controlled by a signal generator. The beam from a 30 mW He-Ne laser (@ 632.8 nm) is split into two different intensity beams by a variable beam splitter. The reflected beam (e.g. object beam) reflects off a steering mirror, is expanded and illuminates the surface of the aluminium plate. A lens gathers the diffused light from the plate and sends it to the beam splitter cube to interfere with the reference beam. The transmitted beam (e.g. reference beam) is reflected off three steering mirrors (e.g. in order to obtain the path length equal with that of the object beam), expanded and sent to the beam splitter cube to interfere with the object beam. The interference pattern is recorded at the CCD.

We adjust the intensities in the two beams such that they have comparable intensities at the CCD. This is to obtain an optimum contrast of the interference pattern. Also, having the 11 cm focal length lens, the dimension of the (subjective) speckle is adjusted with an iris placed just after it, according to the formulae [8, 9]:

$$\sigma_{x,z} = 1.22\lambda f_{\#} \quad \text{and} \quad \sigma_y = 8\lambda f_{\#}^2, \tag{1}$$

where λ is the wavelength of the laser and $f_{\#}$ is the numerical aperture of the imaging system (e.g. lens/iris).

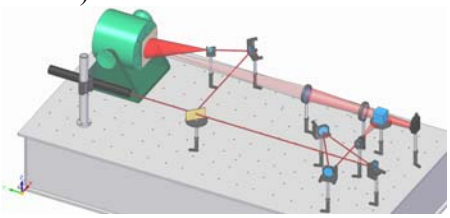

Fig. 1. DSPI experimental setup.

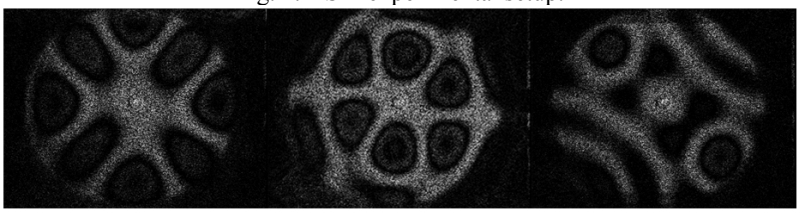

Fig. 2. Speckle interferograms obtained by subtracting two instances in during the vibration of the plate. The 3.05, 4.18 and 4.56 kHz vibration modes are shown.

Speckles of 35.09 nm in the x, z directions (e.g. plane of the plate; see Fig. 1 to visualize the reference system) and 10.45 nm in the y direction (e.g. perpendicular to the plate) were obtained, with our setup.

To obtain the speckle interferograms, we record two instances during the vibration of the plate and subtract the images. Thus, the nodes of the vibration will appear dark as the phase difference will not change during vibration (Fig. 2). The moving parts of the plate will appear gray as the phase difference is changing during the vibration. So, by subtracting two speckle interferograms recorded at different times during the vibration cycle, not only we make a time-average we also get an improvement of the contrast. However, further image processing is needed to improve de *SNR* of the speckle interferograms.

3. Processing of speckle interferograms

There are two categories of image enhancement techniques: spatial domain methods and frequency domain methods. The spatial domain refers to the image plane itself, the approaches in this category are based on direct manipulation of pixels in an image. Frequency domain methods are based on modifying the Fourier transform of an image.

Our algorithm for improving the *SNR* of the speckle interferograms is applied in the spatial domain and has the following steps:

a) apply a *median filter* (with filter aperture of 3);
b) apply *despeckle filter*;
c) adjust brightness and contrast;
d) estimate the background illumination; subtract the background illumination;
e) adjust contrast;
f) *image averaging* by addition of the initial speckle interferogram;
g) apply *edge preserving smooth filter* (with an amount of smoothing of 3);
h) apply *Gaussian blur filter* (with a radius of 0.6);
i) apply *median filter* (with filter aperture of 3)
j) perform *histogram equalization*.

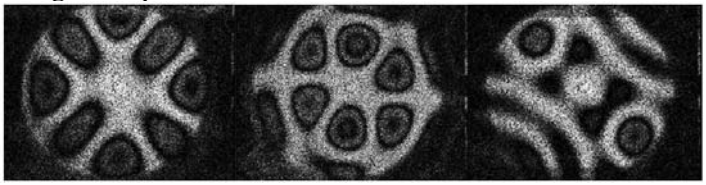

Fig. 3. Speckle interferograms with improved *SNR*. Only steps of the algorithm from a) to i) are applied to these interferograms.

The resulting filtered images are shown in Fig. 3.The *median filter* (Fig. 4) [14, 15], applied in our filtering algorithm, is normally used to reduce noise in an image, somewhat like the mean filter. However, it often does a better job than the mean filter of preserving useful detail in the image. The main idea of the median filter is to run through the signal entry by entry, replacing each entry with the median of neighboring entries. The pattern of neighbors is called the “aperture”,

which slides, entry by entry, over the entire signal. If a pixel contains an extreme value, it is replaced by a "reasonable" value, the median value in the neighborhood. Given a sample of $X_1, \ldots, X_N$ pixels and reordering them so that $Y_1 < Y_2 < \ldots < Y_N$, then Y_i is called the i^{th} order statistic.

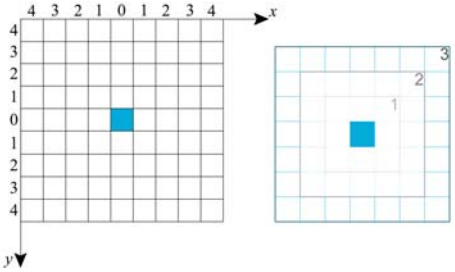

Fig. 4. The pattern of pixels called aperture. The median filter is applied to the central pixel of the given aperture, for each pixel at the time.

Now, given the order statistic $Y_1 = \min_j X_j$, Y_2, …, Y_{N-1}, $Y_N = \max_j X_j$, the statistical median of the random sample is defined by:

$$\tilde{x} = \begin{cases} Y_{(N+1)/2} & \text{if } N \text{ is odd} \\ \frac{1}{2}\left(Y_{N/2} + Y_{1+N/2}\right) & \text{if } N \text{ is even} \end{cases}. \tag{2}$$

Thus, a median filter having an aperture of 3 will result in 8 neighboring pixels. Larger neighborhoods will produce more severe smoothing, but will reduce the information in the image at the same time.

The *despeckle filter* [14, 16] removes noise from images without blurring edges. It attempts to detect complex areas and leave them intact, while smoothing areas where noise will be noticeable.

The effect is that grain or other noise is reduced without severely affecting edges. Standard deviation of each pixel and its neighbors is calculated to determine if the area is one of high or low complexity. If the complexity is lower than the threshold, the area is smoothened using a simple mean filter.

Image averaging [14] by adding the initial noisy image to the image with a degree of filtration, at this stage. Consider a noisy image $g(x, y)$ formed by the addition of noise $h(x, y)$ to an original image $f(x, y)$; that is,

$$g(x, y) = f(x, y) + \eta(x, y), \tag{3}$$

with the assumption that at every pair of coordinates (x, y) the noise is uncorrelated (e.g. has zero covariance with respect to the mean value) and has zero average value. This procedure wants to reduce noise by adding a set of noisy images $g_i(x,y)$, in our case one image. Thus, an image $\bar{g}(x, y)$ is formed by averaging K different noisy images:

$$\bar{g}(x, y) = \frac{1}{K}\sum_{i=1}^{K} g_i(x, y). \tag{4}$$

It follows that

$$E\{\bar{g}(x,y)\} = f(x,y), \text{ and} \tag{5}$$

and

$$\sigma^2_{\bar{g}(x,y)} = \frac{1}{K}\sigma^2_{\eta(x,y)}, \tag{6}$$

where $E\{\bar{g}(x,y)\}$ is the expected value of $\bar{g}$, while $\sigma^2_{\bar{g}(x,y)}$ and $\sigma^2_{\eta(x,y)}$ are the variances of $\bar{g}$ and η respectively, all computed at coordinates (x, y). The standard deviation at any point in the average image is

$$\sigma_{g(x,y)} = \frac{1}{\sqrt{K}}\sigma_{\eta(x,y)}. \tag{7}$$

Equations (6) and (7) indicate that noise of the pixel values at each location (x, y) decreases as K increases. Moreover, the equality in equation (5), suggests that $\bar{g}(x,y)$ approaces $f(x, y)$ as the number of noisy images used in the averaging process increases. We used only two images as to keep the inevitable introduction of blurring in the output image to a minimum.

Nonlinear filters locate and remove data that is recognized as noise. The algorithm is called nonlinear because it looks at each data point and decides if that data is noise or valid signal. If the point is noise, it is simply removed and replaced by an estimate based on surrounding data points, and parts of the data that are not considered noise are not modified at all. Linear filters, such as those used in bandpass, highpass, and lowpass, lack such a decision capability and therefore modify all data. Nonlinear filters are sometimes used also for removing very short wavelength, but high amplitude features from data.

The *edge preserving smooth filter* [14] is also a nonlinear filter and is based on the Kuwahara algorithm [17, 18]. The algorithm implies that for a gray level image $I(x,y)$ and a square patch of the image centered on a pixel of (x, y) coordinates, this area can be divided into four identical squares (Fig. 5*a*) P_1, P_2, P_3, and P_4, with the coordinates:

$$\begin{aligned} P_1(x,y) &= [x, x+d]\times[y, y+d] \\ P_2(x,y) &= [x-d, x]\times[y, y+d] \\ P_3(x,y) &= [x-d, x]\times[y-d, y] \\ P_4(x,y) &= [x, x+d]\times[y-d, y] \end{aligned}, \tag{8}$$

where "×" denotes the Carthesian product. Now, let $m_i(x, y)$ and $\sigma_i(x, y)$ be the local average and local standard deviation respectively, computed on each square $P_i(x, y)$, i = 1,…4. For a given point (x, y), the output $I_K(x,y)$ of the Kuwahara filter is given by the vaule of $m_i(x, y)$ that correesponds to the i-th square providing the minimum value of $\sigma_i(x, y)$ [18]. This can be sumarized as:

$$I_K(x,y)=\sum_i m_i(x,y)f_i(x,y) \quad \text{where} \quad f_i(x,y)=\begin{cases}1, & \sigma_i(x,y)=\min\limits_k\{\sigma_k(x,y)\}\\ 0, & \text{otherwise}\end{cases} \tag{9}$$

Fig. 5*b* shows the behavior of the Kuwahara operator in the proximity of an edge. When the central point (x, y) is on the dark side of the edge (point A), the chosen value of m_i corresponds to the square that completely lies on the dark side (e.g. P_4), because it is the most homogeneous area, corresponding to minimum σ_i.

On the other hand, as soon as the point (x, y) moves to the bright side (point B), the output is determined by the square that lies entirely in the bright area (e.g. P_2). This flipping mechanism guarantees the preservation of edges and corners, while the local averaging smoothes out texture and noise.

The *Gaussian blur* [14, 19] is a linear filter that gets rid of the Gaussian noise in the image. The shape and dimension of the filter must take into account the standard deviation of the noise that affects the image:

$$G(x,y)=\frac{1}{2\pi\sigma^2}e^{-\frac{\left((x-x_0)^2+(y-y_0)^2\right)}{2\sigma^2}}, \tag{10}$$

where σ is the standard deviation, (x_0, y_0) are the coordinats of the central row and column of the kernel (e.g. Fig. 4), and (x, y) are the coordinates of the pixel to which the filter is applied.

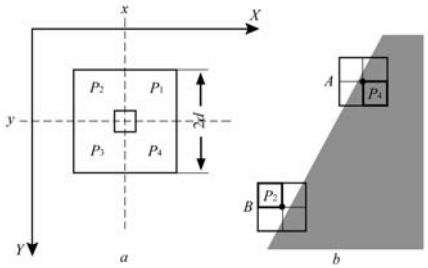

Fig. 5. Kuwahara filtering (Edge Preserving Smooth): a – P_i regions on which local averages and standard deviations are computed; b – Region of smallest standard deviation (shown by a thick line) determines the output of the filter.

The image restoration is, then, realized by the convolution of the source image with the previously computed Gaussian kernel/filter, such that:

$$I_D(x,y)=G(x,y)*I_S(x,y), \tag{11}$$

where I_D (x, y) is the filtered image and I_S (x, y) is the source image.

However, when the dimension of the filter w is large, the convolution operation may be time consumming. In this case, we can use the separabilty property (Fig. 6) of the Gaussian function:

$$G(x,y)=G(x)G(y), \tag{12}$$

and replace the convolution with a bidimensional kernel with two convolutions of one dimensional kernels:

$$I_D(x,y) = (G(x)G(y)) * I_S(x,y) = G(x) * (G(y) * I_S(x,y)), \tag{13}$$

where $G(x)$ and $G(y)$ are the central row and column vectors (Fig. 6) of the bidimensional kernel, namely:

$$G(x) = \frac{1}{\sqrt{2\pi\sigma}} e^{\frac{-(x-x_0)^2}{2\sigma^2}} \quad \text{and} \quad G(y) = \frac{1}{\sqrt{2\pi\sigma}} e^{\frac{-(y-y_0)^2}{2\sigma^2}}. \tag{14}$$

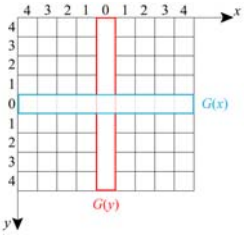

Fig. 6. The two vector components, $G(x)$ and $G(y)$ in which a2D Gaussian kernel can be separated.

The higher the radius of the filter the higher the amount of smoothing.

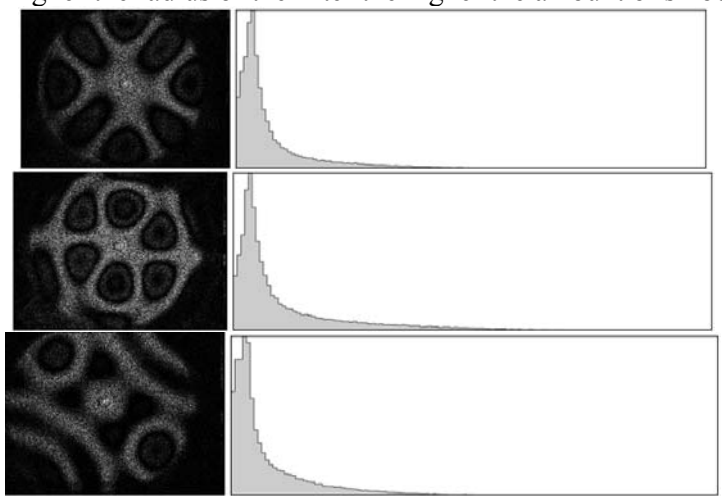

Fig. 7. Speckle interferograms with their corresponding histograms. Notice the poor contrast and dynamic range.

Moreover, aplying multiple, successive Gaussian blurs to an image has the same effect as applying a single, larger Gaussian blur, whose radius is the square root of the sum of the squares of the blur radii that were actually applied. For example, applying successive Gaussian blurs with radii of 3 and 4 gives the same results as applying a single Gaussian blur of radius 5, since $\sqrt{3^2 + 4^2} = 5$. Because of this relationship, processing time cannot be saved by simulating a Gaussian

blur with successive, smaller blurs – the time required will be at least as great as performing the single large blur. On the other hand, Gaussian blurs have nice properties, such as having no sharp edges, and thus do not introduce ringing into the filtered image.

The *histogram equalization* [14, 20] technique is usually used for digitized images composed mostly of pixels with either very dark or very bright gray level components. The probability of occurrence of gray level r_k in an image is approximated by:

$$p_r(r_k) = \frac{n_k}{n} \qquad \text{where} \quad k = 0,1,2,..., L-1, \tag{15}$$

where n is the total number of pixels in the image, n_k is the number of pixels that have gray level r_k , and L is the total number of possible gray levels (e.g. $256 = 2^8$) in the image.

Shortly, the histogram equalization or linearization si given by the transformation:

$$s_k = T(r_k) = \sum_{j=0}^{k} p_r(r_j) = \sum_{j=0}^{k} \frac{n_j}{n} = \qquad \text{where} \quad k = 0,1,2,..., L-1. \tag{16}$$

Thus, a processed image is obtained by mapping each pixel with level r_k in the input image into a corresponding pixel with level s_k in the output image via equation (16). Histogram equalization automatically determines a transformation function that seeks to produce an output image that has a uniform histogram. Histograms of all speckle interferograms are presented, both initial (Fig. 7) and filtered with our algorithm (Fig. 8).

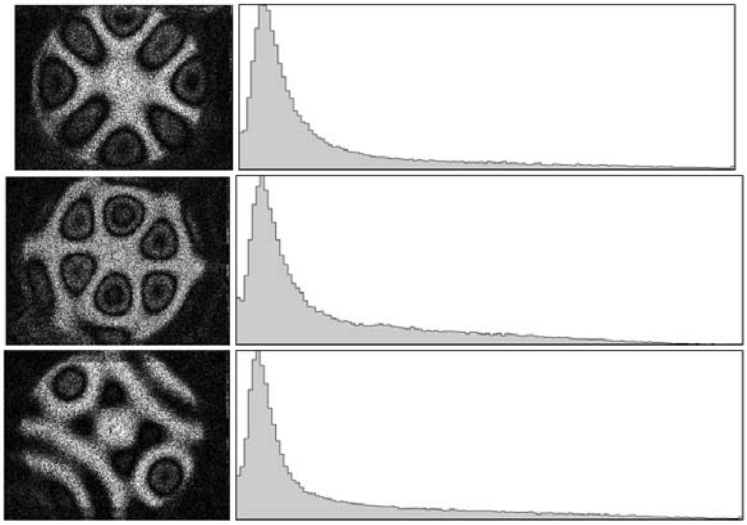

Fig. 8. Filtered speckle interferograms with the corresponding histograms. An improvement in both contrast and dynamic range is noticed.

The initial images have poor contrast and darker pixels. An improvement, regarding the contrast and dynamic range, is noticed for the processed

interferograms. However, the histogram equalization process (Fig. 9) further improves these images.

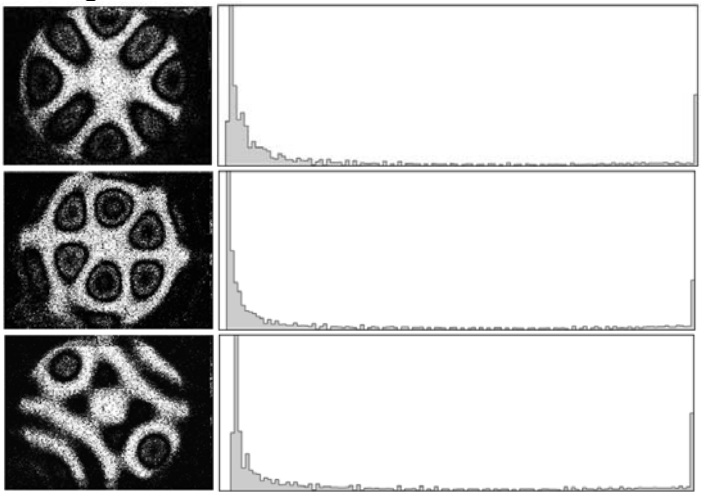

Fig. 9. Speckle interferograms with the corresponding histograms after the histogram equalization was applied. The contrast is greatly enhanced and the dynamic range extended.

In order to estimate the improvement in filtered interferograms we calculated the speckle index and the *SNR*. The speckle index (also called coefficient of variation in image processing language) is the ratio of standard deviation of intensity to the mean of intensity $C = \sigma/m$ and the *SNR* is defined as the inverse of this index $SNR = 1/C$. For the three speckle interferograms we have the following improvement of the *SNR*: 0.3 (for 3.05 kHz), 0.5 (for 4.18 kHz) and 0.3 (for 4.56 kHz).

4. Conclusions

Unlike specular interferometry where the fringes are clear and discernible, in the case of speckle interferograms, post-processing is needed. Processing of these speckle interferograms in the spatial domain to improve *SNR* was presented. An algorithm that uses both linear and nonlinear filters was realized and the speckle interferograms showed an improvement, when applied. We noticed that with this filtering method the *SNR* of the interferograms improved by a factor between 0.3 and 0.5 depending on the vibration mode. For further enhancement of the images, we also used histogram equalization. Thus, both the contrast and dynamic range were improved. Detailed mathematical explanation of the filters we applied was also presented.

REFERENCES

[1] *P. K. Rastogi*, Editor, Digital speckle pattern interferometry and related techniques, Wiley Ed., 2001;

[2] *C.H. Huang*, "Experimental measurements by an optical method of resonance frequencies and mode shapes for square plates with rounded corners and chamfers", J Sound Vib., **vol. 253**, 2002, pp. 571–583;
[3] *C. H. Huang and C. C. Ma*, "Vibration characteristics for piezoelectric cylinders using amplitude fluctuation electron speckle pattern interferometry", Am. Inst. Aeronaut. Astronaut. J., **vol. 36**, 1998, pp. 2262–2268;
[4] *U.M. Chaudhari, A.R. Ganeshan, C. Shakher, P.B. Godbole and R.S. Sirohi*, "Investigation on in plane stresses on bolted flanged joints using digital speckle pattern interferometry", Opt. Laser Eng., **vol. 11**, 1989, pp. 257-264;
[5] *R. Kumar, I.P. Singh and C. Shakher*, "Measurement of out-of-plane static and dynamic deformations by processing digital speckle pattern interferometry fringes using wavelet transform", Opt. Laser Eng., **vol. 41**, 2004, pp. 81-93;
[6] *R. Kumar, S.K. Singh and C. Shakher*, "Analysis of small vibrations of computer hard disk surface using digital speckle pattern interferometry and wavelet thresholding", Opt. Laser Technol., **vol. 33**, 2001, pp. 567-571;
[7] *C. Shakher, R. Kumar, S.K. Singh and S.A. Kazmi*, "Application of wavelet filtering for vibration analysis using digital speckle pattern interferometry", Opt. Eng., **vol. 41**, 2002, pp. 176-180;
[8] *Angelica Svanbro*, Speckle Interferometry and Correlation Applied to Large-Displacement Fields, PhD Thesis, Luleå University of Technology, Sweden, 2004;
[9] *J. C. Dainty*, Laser Speckle and Related Phenomena, Springer-Verlag, 1975;
[10] *S. Mirza, P. Singh, R. Kumar, A. L. Vyas and C. Shakher*, "Measurement of transverse vibrations/visualization of mode shapes in square plate by using digital speckle pattern interferometry and wavelet transform", Optics and Lasers in Engineering, **vol. 44** (1), 2006, pp. 41-55;
[11] *T. R. Crimminis*, "Geometric Filter for Speckle Reduction", Appl. Opt., **vol. 24**, 1985, pp. 1438-1443;
[12] *S. Mirza, R. Kumar and C. Shaker*, "Study of various processing schemes and wavelet filters for speckle noise reduction in digital speckle pattern interferometric fringes", Opt. Eng., **vol. 44**, 2005, pp. 045603;
[13] *C. Loizou, C. Christodoulou, C. S. Pattichis, R. Istepanian, M. Pantziaris and A. Nicolaides*, "Speckle reduction in ultrasound images of atherosclerotic carotid plaque", IEEE 14th International Conference on Digital Signal Processing, 2002, pp. 1-4;
[14] *C. Gonzales and R. E. Woods*, Digital image processing, Prentice Hall, Inc. 2002;
[15] *I. Pitas and A. N. Venetsanopoulos*, "Nonlinear digital filters: principles and applications", Kluwer Academic, 1990
[16] *B. Priestly Shan and M. Madheswaran*, "A generalized despeckling filter for enhancing fetal structures to aid automated obstetric pathologies", International Journal of Computer Theory and Engineering, **vol. 2** (3), 2010, pp. 445-453;
[17] *M. Kuwahara, K. Hachimura, S. Ehiu and M. Kinoshita*, "Processing of ri-angiocardiographic images", K. Preston and M. Onoe, Ed. 1976, Plenum Press, New York, pp. 187-203;
[18] *G. Papari, N.Petkov and P. Campisi* "Artistic edge and corner enhancing smoothing", IEEE Transactions on Image Processing, **vol. 29** (10), 2007, pp. 2449-2462;
[19] *R. Haralick and L. Shapiro*, Computer and robot vision, Addison-Wesley Publishing Company, 1992, Vol. 1, Chap. 7;
[20] *M. Rosu, B. Ionita, D. Apostol, F. Garoi and P. C. Logofatu*, "Histogram equalization and specification in interferometry", J. Optoelectron Adv. Mat. – Rapid Communications, **vol. 3** (4), 2009, pp. 376-378.